

# Line-Charge-Mediated Concentration Enrichment in Continuous Shear Flow toward Portable Membrane-Free Water Purification

Peng Huo,<sup>#</sup> Wei Liu,<sup>#</sup> Zhibo Gu, Moran Wang,<sup>\*</sup> and Daosheng Deng<sup>\*</sup>



Cite This: <https://doi.org/10.1021/acs.nanolett.5c04366>



Read Online

ACCESS |



Metrics & More



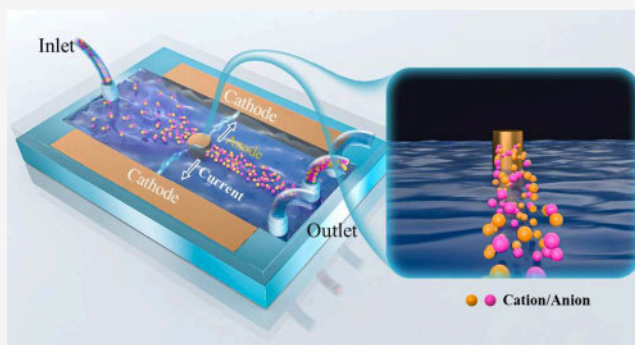
Article Recommendations



Supporting Information

**ABSTRACT:** The purification and treatment of water have assumed greater significance in the context of sustainable development. Nevertheless, the conventional theory of concentration polarization inherently imposes constraints on the effective regulation and precise manipulation of ionic transport for electrochemical-based technology. In this work, we propose an extraordinary concentration enrichment mediated by a line charge down to tens of micrometers, allowing continuous extraction in shear flow. The spatiotemporal evolution of the solute concentration is experimentally observed under various applied voltages and flow rates in a microfluidic-based electrochemical device. Through numerical simulations and scaling analysis, we elucidate the trade-offs between key physical parameters to optimize enrichment performance. Furthermore, we demonstrate the effective removal of plastic particles and cells in solutions. This portable water purification concept may extend options for drinking water access in disaster response or infrastructure-constrained environments.

**KEYWORDS:** Concentration enrichment, Line charge, Shear flow, Water purification



the cation separation in multicomponent electrolytes and the effective removal of plastic particles and cells in solutions. This portable water purification concept may extend options for drinking water access in disaster response or infrastructure-constrained environments.

Water purification, encompassing desalination, decontamination, and disinfection, has become increasingly crucial in addressing the challenge of inadequate access to clean water, which is essential for global sustainable development.<sup>1–4</sup> From the perspective of practical applications, mainstream desalination technologies, such as the state-of-the-art methods of reverse osmosis and electrodialysis, heavily rely on membranes. These membranes come with a range of disadvantages, including the membranes' susceptibility to mechanical fragility, degradation due to chemical exposure, fouling by biological matter, the necessity for periodic replacement, and the trade-off between permeability and selectivity.<sup>5–8</sup> Capacitive deionization technology facilitates the selective adsorption of diverse ionic species through the manipulation of surface-functionalized electrode materials, but its ion-removal capacity is constrained prior to the necessitated reactivation and rejuvenation of the carbon electrode matrices.<sup>9–11</sup> By dissolving CO<sub>2</sub> into water, the diffusio-phoresis of colloidal particles, driven by ion concentration gradients resulting from dissociation, enables a continuous flow and membraneless particle filtration process.<sup>12</sup>

From the perspective of fundamental science, ion transport in electrolytes is essential for the operation and performance of desalination and, more broadly, water treatment.<sup>13,14</sup> When ions are subjected to electromigration and diffusion across a perfectly ion-selective interface in a wide spectrum of electrochemical technological scenarios (such as cation- and

anion-selective membranes or charged nanochannels,<sup>15,16</sup> nanotubes<sup>17</sup>), the classical theory of concentration polarization, formulated by Levich in the 1940s, suggests that an initially dilute binary electrolyte with a concentration ( $c_0$ ) placed between parallel electrodes, in the absence of convection, will exhibit a linear distribution of concentration in the spatial domain.<sup>18–20</sup> Consequently, at the diffusion-limited current, the concentration at the cathode is depleted to zero, while at the anode, it becomes enriched to a maximum ( $c_{max} = 2c_0$ ), indicating an upper bound of the enrichment factor ( $f_{enrich} = c_{max}/c_0 = 2$ ) as a key performance metric.

Significant progress has been made in the investigation of the depletion region, such as the Rubinstein–Zaltzman electroconvection instability arising from the extended space charge.<sup>21–24</sup> As the analyte samples, such as the charged particles, in the buffer solutions drift by the amplified electric field in the depletion, the million-fold preconcentration is trapped near the cathode for biomolecule separation and seawater desalination.<sup>25,26</sup> In the microchannels, the surface

**Received:** August 27, 2025

**Revised:** October 2, 2025

**Accepted:** October 3, 2025

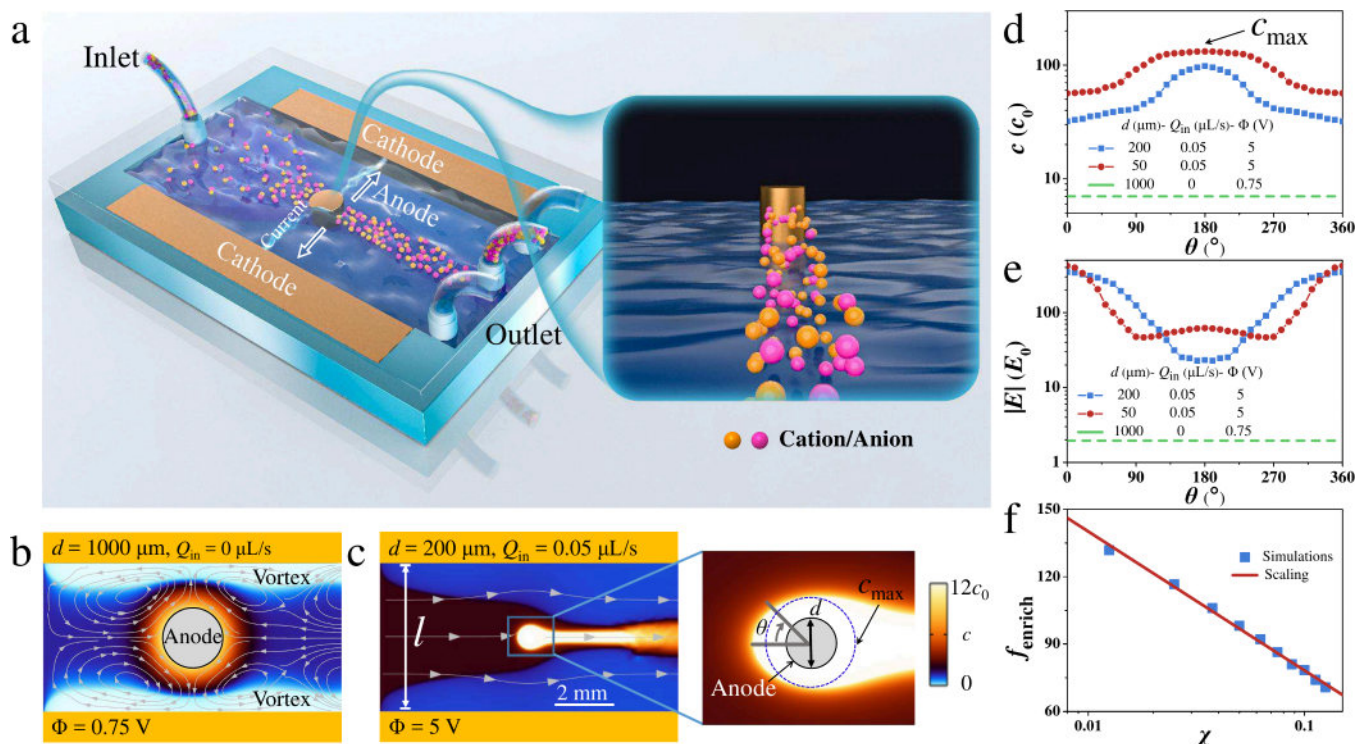


**Figure 1.** Sketch and principle of the device. (a) Sketch of the quasi-two-dimensional microfluidic-based electrochemical device. The upstream inlet for the feeding solution to be treated; three downstream outlets for the draining solution, the middle one for the extraction of enrichment solution, while two side outlets for the discharge of the residual diluted solution. (b, c) Simulation snapshot for the concentration distribution and flow field without the shear flow at a moderate voltage and with the shear flow at a high voltage, respectively. (d, e) Azimuthal dependence of concentration and the magnitude of electric field at various physical parameters. (f) Scaling of  $f_{\text{enrich}} \sim -\ln \chi$  ( $Q_{\text{in}} = 0.05 \mu\text{L/s}$ ,  $\Phi = 5 \text{ V}$ ,  $l = 4 \text{ mm}$  in simulations).

charge can pronouncedly affect the ion transport in the depletion region, leading to the propagation of the deionization shock for shock electro dialysis.<sup>27–31</sup> However, in the concentration enrichment, the upper bound of the enrichment factor near the anode continues to impose a fundamental physical constraint on theoretical models, inherently hindering the efficiency and performance of related technologies.

In order to transcend the theoretical upper bound and investigate alternative membrane-free technology, in this work we propose the extraordinary concentration enrichment driven by the line charge (or line current) down to a reduced length scale of tens of micrometers and the continuous cation separation and extraction in continuous shear flow. Experimentally we build a quasi-two-dimensional microfluidic electrochemical device by placing a central cylindrical anode between parallel cathodes and directly observe the spatiotemporal evolution of concentration, signifying an extraordinary  $f_{\text{enrich}}$ . Numerical simulations reveal the underlying mechanism of line-charge-mediated enrichment and show an excellent agreement with experiments. Additionally, the scaling law for  $f_{\text{enrich}}$  elucidates the trade-offs between key physical parameters, providing insights for the optimization operation. Furthermore, we demonstrate the preferential cation enrichment and depletion in multicomponent electrolytes and the removal of plastic particles and biological cells for water treatment. This portable water purification concept may extend options for drinking water access alongside large-scale desalination, including in disaster response or infrastructure-constrained environments.

## SKETCH AND PRINCIPLE FOR THE DEVICE

As illustrated in Figure 1a, we design and construct a microfluidic-based electrochemical device with a thickness of  $h = 30 \mu\text{m}$ , the central anode with diameter  $d \sim 200 \mu\text{m}$  ( $\Phi \sim 10 \text{ V}$ ), and the distance between two cathodes  $l = 4 \text{ mm}$ . The shear flow ( $Q_{\text{in}} \sim 0.1 \mu\text{L/s}$ ) is applied via the upstream and downstream between two parallel cathodes, consequently facilitating the continuous separation and extraction of the treated solution. Differing from the bipolar electrode configuration that utilizes parallel electrodes for the cathode and anode,<sup>32–35</sup> the configuration presented here features a central anode for concentration enrichment alongside two parallel plate cathodes. To the best of our knowledge, this configuration featuring a line-charged electrode is the first of its kind to be used for ion enrichment in water treatment.

The principle of this device is demonstrated by numerical simulations (Figure 1b–f, Supporting Information).<sup>21,22,36–40</sup> Without an external shear flow at a moderated voltage ( $Q_{\text{in}} = 0$ ,  $\Phi = 0.75 \text{ V}$ ) (Figure 1b), the concentration is symmetrically enriched at the central anode, while the electro-osmotic instabilities of concentration depletion as indicated by the white streamlines appear.<sup>40</sup> However, with an applied shear flow at a strong voltage ( $Q_{\text{in}} = 0.05 \mu\text{L/s}$ ,  $\Phi = 5 \text{ V}$ ), the concentration distribution around the central circular anode becomes directionally dependent and varies with the azimuthal angle [ $c(\theta)$ ] (Figure 1c,d), and the maximum concentration [ $c_{\text{max}} = c(\theta = 180^\circ)$ ] occurs along the downstream direction. Also the magnitude of the electric field around the central anode exhibits directional characteristics (Figure 1e).

Similar to the line charge of a curved geometry,<sup>40</sup>  $f_{\text{enrich}}$  has the following scaling:

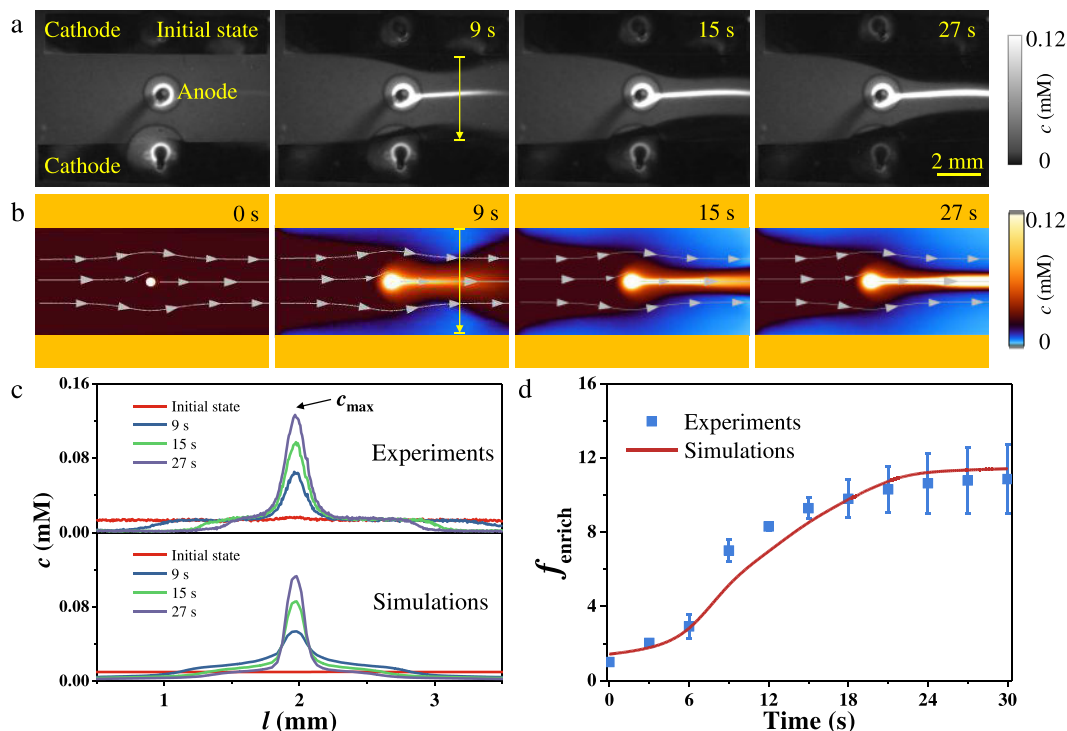


**Figure 2.** Spatiotemporal evolution of concentration enrichment under the continuous operation of shear flow. (a) Experiment of concentration evolution of fluorescence dye. (b) Simulation of the concentration evolution and white arrows for the flow velocity ( $Q_{in} = 0.2 \mu\text{L/s}$ ,  $\Phi = 10 \text{ V}$ ,  $d = 200 \mu\text{m}$ ). (c) The concentration profile across the two parallel cathodes along the yellow line in the downstream in experiments and  $c_{max}$  for the central peak concentration. (d)  $f_{enrich}$  as a function of time and all the error bars for the three measurements in experiments hereafter.

$$f_{enrich} \sim c_{max} = c|_{r=\chi} \sim -\ln \chi \quad (1)$$

where the dimensionless length scale is  $\chi = d/l$  here. This scaling agrees with the simulations remarkably (Figure 1f), and  $f_{enrich}$  tends to become a singularity with  $\chi \rightarrow 0$ . In experiments, as the diameter of the line anode is reduced to the micrometer or nanometer scale, numerous potential nonlinear effects (such as electrode reactions and others) can make the phenomenon challenging to control and observe clearly.

The dimensionless Peclet number,  $Pe = u_{shear}d/D \sim 10^2 \gg 1$ ,<sup>41</sup> suggests the shear flow becomes pronounced to dominate the ion transport. Indeed, as shown in Figure 1c, the complicated electro-osmotic instability at the anode and cathode has been suppressed by the strong shear flow, considerably simplifying the experiments and simulations here.<sup>42,43</sup>

## ■ SPATIOTEMPORAL EVOLUTION OF CONCENTRATION ENRICHMENT

In order to directly observe the spatiotemporal evolution of concentration, an ionic compound (Alexa Fluor 488 fluorescent dye, Thermo Fisher Scientific) at  $c_0 = 0.01 \text{ mM}$  is injected upstream ( $Q_{in} = 0.2 \mu\text{L/s}$ ,  $\Phi = 10 \text{ V}$ , Figure 2a, Supplementary Video 1). In this central anode and parallel-plate cathode system, water electrolysis is suppressed and no bubbles are observed during operation at the given voltage (Supporting Information). Initially at  $t = 0 \text{ s}$ , the distribution of fluorescence intensity from the anions is nearly homogeneous, but after applying the voltage at  $t = 9 \text{ s}$ , the concentration depletion is formed near the region of the cathode, while the concentration enrichment occurs near the vicinity of the central anode (the fluorescent intensity increases

linearly with concentration in accordance with the calibration curve, Supporting Information). Subsequently at  $t = 15 \text{ s}$ , both depletion and enrichment are further developed. Eventually, at  $t = 27 \text{ s}$ , a brighter enrichment zone is produced in the downstream flow. Numerical simulations of concentration evolution are comparable to the experiments (Figure 2b, Supplementary Video 2).

Quantitatively, for the concentration distribution across the two parallel cathodes downstream (along the yellow line in Figure 2a,b), simulations and experiments agree excellently (Figure 2c).  $f_{enrich}$  rises over time and stabilizes at approximately  $12.4 \pm 2.2$  after  $t = 24 \text{ s}$ , clearly exhibiting a remarkable enrichment effect of more than 1 order of magnitude (Figure 2d). When a platinum electrode is used as the central anode, a similar concentration enrichment is also observed (Supporting Information).

## ■ ENRICHMENT PERFORMANCE DEPENDENT ON OPERATION PARAMETERS

We further investigate the effect of the various physical parameters, such as the applied voltage ( $\Phi$ ) and inflow rate ( $Q_{in}$ ), on the enrichment performance ( $f_{enrich}$ ). The snapshot (Figure 3a) and concentration distribution at the downstream (Figure 3b) in both experiments and simulations reveal that concentration enrichment becomes more pronounced at a higher voltage at a given flow rate. Also the enrichment performance turns out to be less at a stronger flow rate, as the ions have more tendency to be swept away by the flow with insufficient time to be accumulated.

The enrichment performance  $f_{enrich}$  dependent on  $\Phi$  and  $Q_{in}$  is demonstrated in experiments (Figure 3c) and simulations

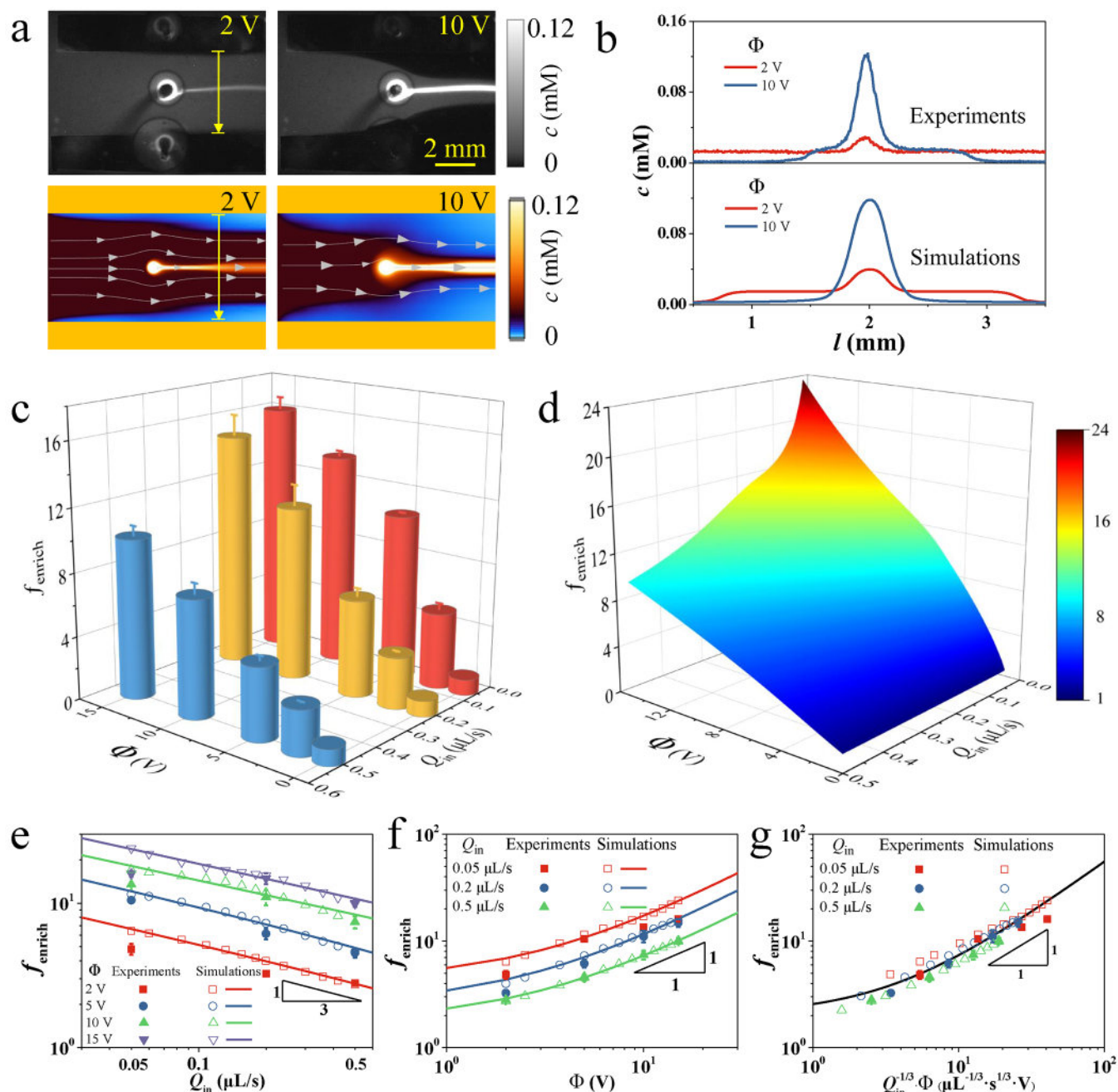


**Figure 3.** Enrichment factor dependent on voltages and inflow rates. (a) Snapshot of experiments and simulations at  $t = 30$  s ( $Q_{\text{in}} = 0.2 \mu\text{L/s}$ ). (b) Concentration profile along the yellow line in the downstream. (c, d)  $f_{\text{enrich}}$  as a function of  $\Phi$  and  $Q_{\text{in}}$  in experiments (c) and simulations (d). Scaling law for (e)  $f_{\text{enrich}} \sim Q_{\text{in}}^{-1/3}$ , (f)  $f_{\text{enrich}} \sim \Phi$ , and (g)  $f_{\text{enrich}} \sim Q_{\text{in}}^{-1/3} \Phi$ .

(Figure 3d). As shown in Figure 3c,  $f_{\text{enrich}}$  can be increased to  $15.6 \pm 0.8$  at a higher  $\Phi = 15$  V and a lower  $Q_{\text{in}} = 0.05 \mu\text{L/s}$ , as confirmed by simulations. Thus, by adjustment to a higher voltage or a lower flow rate, a better enrichment can be achieved. Treatment capability of extraction solution per unit time decreases at a lower flow rate, indicating a trade-off between the flow rate and the enrichment performance.

**Scaling Analysis for  $f_{\text{enrich}}$ .** In order to provide physical insight into  $f_{\text{enrich}}$ , we perform scaling analysis dependent on the physical parameters and operation conditions ( $Q_{\text{in}}$  and  $\Phi$ ). By combining concentration flux ( $c_{\text{enrich}} \sim \Phi$ ) and flow effect ( $c_{\text{enrich}} \sim Q_{\text{in}}^{-1/3}$ )<sup>44</sup> (Supporting Information), the following scaling is obtained:

$$f_{\text{enrich}} \sim Q_{\text{in}}^{-1/3} \Phi \quad (2)$$

Both experiments and simulations agree with this scaling law excellently (Figure 3e–g). At a fixed voltage, we find that  $f_{\text{enrich}}$  has a  $-1/3$  power law with  $Q_{\text{in}}$  (Figure 3e); at a fixed flow rate,  $f_{\text{enrich}} \propto \Phi$  (Figure 3f). As illustrated in Figure 3g, all the data in the experiments and simulations at different  $Q_{\text{in}}$  and  $\Phi$  collapse onto a single line, consistent with the scaling law (eq 2).

**Preferential Enrichment and Reduction of Cations.** After establishing line-charge-mediated concentration enrichment through the direct observation of fluorescent dye concentration, we proceeded to explore the continuous extraction of  $\text{Cu}^{2+}$  enrichment at different  $Q_{\text{in}}$  and  $\Phi$  (Figure

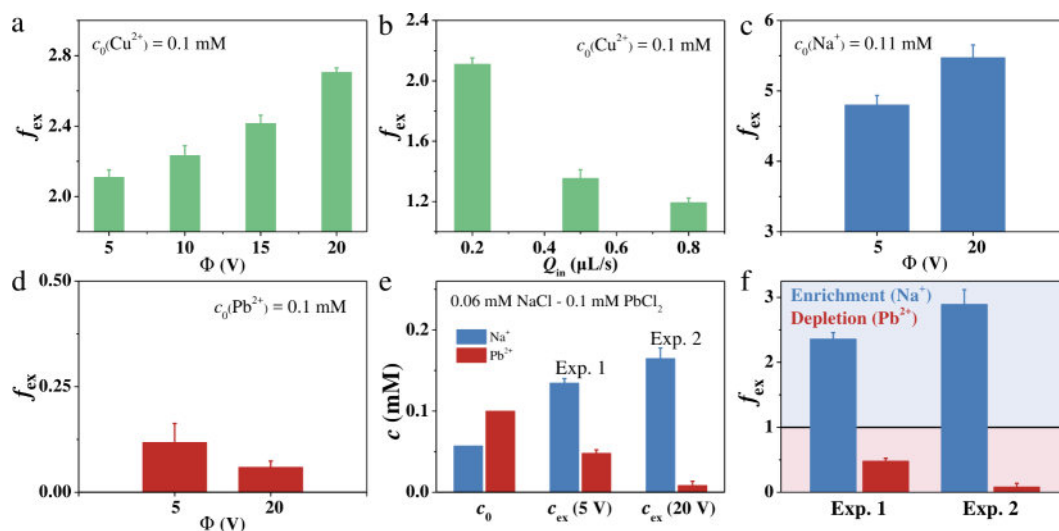


**Figure 4.** Preferential enrichment and reduction of a cation and the separation of cations in multicomponent electrolytes. (a, b)  $f_{ex}$  of  $\text{Cu}^{2+}$  in  $\text{CuSO}_4$  increasing with  $\Phi$  ( $Q_{in} = 0.2$ ,  $Q_{ex} = 0.02 \mu\text{L/s}$ ), but decreasing with  $Q_{in}$  ( $\Phi = 5 \text{ V}$  and  $Q_{ex} = 0.02 \mu\text{L/s}$ ). (c) The enrichment efficiency of  $\text{Na}^+$  in  $\text{NaCl}$  ( $c_0 = 0.11 \text{ mM}$ ) ( $\Phi = 5, 20 \text{ V}$ ,  $Q_{in} = 0.2 \mu\text{L/s}$ , and  $Q_{ex} = 0.1Q_{in}$ ). (d) Concentration reduction of  $\text{Pb}^{2+}$  in  $\text{PbCl}_2$  at  $\Phi = 5$  and  $20 \text{ V}$ . (e) Separation of  $\text{Na}^+$  and  $\text{Pb}^{2+}$  in the mixed solution ( $0.06 \text{ mM NaCl} - 0.1 \text{ mM PbCl}_2$ ) at  $\Phi = 5, 20 \text{ V}$  and (f) for the enriched  $\text{Na}^+$  [ $f_{ex}(\text{Na}^+) > 1$ ] and the depleted  $\text{Pb}^{2+}$  [ $f_{ex}(\text{Pb}^{2+}) < 1$ ].

4a,b). The copper sulfate solution ( $\text{CuSO}_4$ ) at  $c_0 = 0.1 \text{ mM}$  is injected upstream at  $Q_{in} = 0.2 \mu\text{L/s}$ , and the enriched  $\text{Cu}^{2+}$  solution is extracted through the central enrichment outlet in the downstream at the extracted rate  $Q_{ex} = 0.1$ ,  $Q_{in} = 0.02 \mu\text{L/s}$ .  $\text{Cu}^{2+}$  concentration in the extraction solution ( $c_{ex}$ ) is measured quantitatively by inductively coupled plasma optical emission spectrometry (ICP-OES). As  $\Phi$  increases from 5 to 20 V to promote the enrichment effect, the extraction concentration factor ( $f_{ex} = c_{ex}/c_0 > 2$ ) grows with the voltage, exceeding the upper bound in the classical theory of concentration polarization (Figure 4a). Here the dendrite growth near the cathodes at a high voltage  $\Phi = 20 \text{ V}$  is suppressed due to the presence of the incoming shear flow.<sup>43</sup> Also under constant  $\Phi$  and  $Q_{ex}$ ,  $f_{ex}$  decreases with  $Q_{in}$  (Figure 4b), since the strong shear flow and convection at a higher  $Q_{in}$  will reduce the tendency of concentration accumulation near the central anode. Besides metal copper ions ( $\text{Cu}^{2+}$ ), the sodium ions ( $\text{Na}^+$ ) can be enriched and extracted through this line-charge-mediated enrichment with  $f_{ex} \sim 5$  (Figure 4c).

However, under similar operation conditions in experiments, the heavy metal lead ions ( $\text{Pb}^{2+}$ ) and magnesium ions ( $\text{Mg}^{2+}$ ) are depleted in the extracted solution, instead of the enrichment. By injecting a  $c_0 = 0.1 \text{ mM PbCl}_2$  solution in the inlet with  $Q_{in} = 0.2 \mu\text{L/s}$  and  $Q_{ex} = 0.1Q_{in}$ ,  $c_{ex}$  decreased to 0.01 and 0.006 mM at  $\Phi = 5$  and 20 V, corresponding to a 1 order of magnitude reduction of concentration (Figure 4d). This abnormal depletion effect might originate from the formation of insoluble  $\text{Pb}(\text{OH})_2$ , which is produced by the reaction between  $\text{Pb}^{2+}$  and hydroxide ( $\text{OH}^-$ ) generated at the cathode. This insoluble  $\text{Pb}(\text{OH})_2$  is further verified by the progressively larger white precipitate near the cathode in the experiment. Similarly, since  $\text{Mg}^{2+}$  can react with  $\text{OH}^-$  to form insoluble  $\text{Mg}(\text{OH})_2$ ,  $\text{Mg}^{2+}$  exhibited the same depletion effect (Supporting Information).

## ■ CATION SEPARATION IN MULTICOMPONENT ELECTROLYTE SOLUTIONS

Heavy metal pollution, such as lead pollution in natural water, has become a major challenge for water treatment and sustainable environmental development. Typically, the removal of lead ions requires the complex synthesis of the electrode materials or adsorbents,<sup>45</sup> the precipitation filtration,<sup>46</sup> or the electroactive ion exchange composite film.<sup>47</sup>

Here by utilizing preferential enrichment ( $\text{Cu}^{2+}$ ,  $\text{Na}^+$ ) and selective depletion ( $\text{Pb}^{2+}$ ,  $\text{Mg}^{2+}$ ), we might separate the various species of cations in the multicomponent electrolytes effectively. The aqueous multicomponent electrolytes are composed of 0.06 mM  $\text{NaCl}$  and 0.1 mM  $\text{PbCl}_2$  [ $c_0(\text{Na}^+) = 0.06 \text{ mM}$ ,  $c_0(\text{Pb}^{2+}) = 0.1 \text{ mM}$ ]. As seen in Figure 4e, the enriched  $c_{ex}(\text{Na}^+) = 0.14 \text{ mM}$ , while the depleted  $c_{ex}(\text{Pb}^{2+}) = 0.05 \text{ mM}$  ( $\Phi = 5 \text{ V}$ ,  $Q_{in} = 0.2 \mu\text{L/s}$ ,  $Q_{ex} = 0.1$ ,  $Q_{in} = 0.02 \mu\text{L/s}$ ). As  $\Phi = 20 \text{ V}$ , we obtain the further enriched  $c_{ex}(\text{Na}^+) = 0.16 \text{ mM}$  and the further depleted  $c_{ex}(\text{Pb}^{2+}) = 0.008 \text{ mM}$ , indicating that the cation separation becomes more significant at a higher voltage. Clearly, the dimensionless  $f_{ex}$  for both cations (Figure 4f) indicates  $f_{ex}(\text{Na}^+) = c_{ex}(\text{Na}^+)/c_0(\text{Na}^+) > 1$  for the enriched concentration, while  $f_{ex}(\text{Pb}^{2+}) = c_{ex}(\text{Pb}^{2+})/c_0(\text{Pb}^{2+}) < 1$  for the depleted concentration, demonstrating the effective separation of the cations in the extracted solution.

The energy consumption for  $\text{Cu}^{2+}$ ,  $\text{Na}^+$ ,  $\text{Pb}^{2+}$ , and a mixed  $\text{Na}^+ - \text{Pb}^{2+}$  solution is approximately 0.01 kWh/m<sup>3</sup> at low voltage (5 V) and approximately 0.1 kWh/m<sup>3</sup> at high voltage (20 V), which is on the same order of magnitude as shock electro dialysis (Supporting Information).<sup>48</sup> But different from the recently studied shock electro dialysis in which continuous and selective removal of lead in the  $\text{Na}^+ - \text{Pb}^{2+}$  mixed solution arises from the faster transport and the larger escape barrier of lead ions as compared with sodium ions,<sup>48</sup> our approach could reduce  $\text{Pb}^{2+}$  concentration, while elevating  $\text{Na}^+$  concentration, leading to effective selectivity.

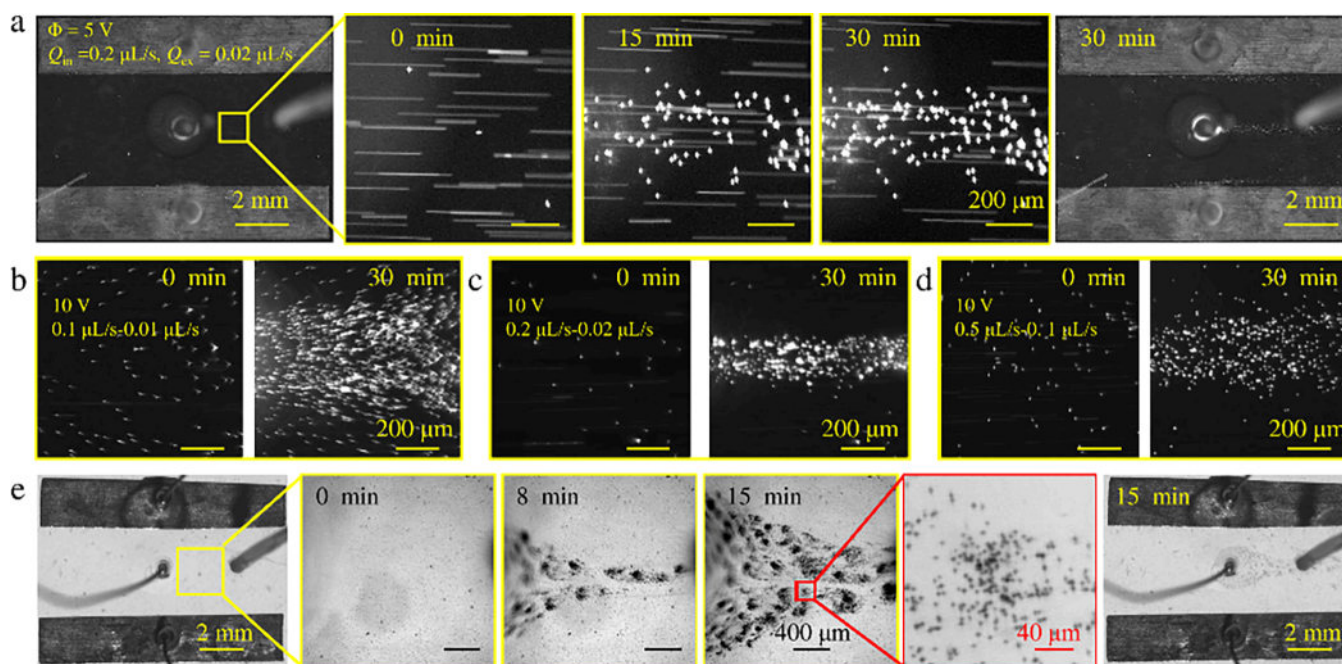


**Figure 5.** Contaminant removal of plastic particles and cells. (a) Spatiotemporal evolution of plastic particles in full view and enlarged view ( $\Phi = 5$  V,  $Q_{in} = 0.2 \mu\text{L/s}$ ,  $Q_{ex} = 0.02 \mu\text{L/s}$ ). (b–d) Particle aggregation at (b)  $\Phi = 10$  V,  $Q_{in} = 0.1 \mu\text{L/s}$ ,  $Q_{ex} = 0.01 \mu\text{L/s}$ ; (c)  $\Phi = 10$  V,  $Q_{in} = 0.2 \mu\text{L/s}$ ,  $Q_{ex} = 0.02 \mu\text{L/s}$ ; (d)  $\Phi = 10$  V,  $Q_{in} = 0.5 \mu\text{L/s}$ ,  $Q_{ex} = 0.1 \mu\text{L/s}$ . (e) Spatiotemporal evolution of cells of *Chlorella* sp. in full view and enlarged view ( $\Phi = 5$  V,  $Q_{in} = 0.2 \mu\text{L/s}$ ,  $Q_{ex} = 0.02 \mu\text{L/s}$ ).

## REMOVAL OF PLASTIC PARTICLES AND CELLS

These devices facilitate microplastic capture in compact water-quality monitors<sup>49–51</sup> and the removal of bacteria or cells in biomedical/chemical sensors.<sup>52,53</sup> A suspension of 3.2  $\mu\text{m}$  fluorescent polystyrene particles (PS) (Thermo Fisher Scientific,  $10^{-5}$  mass ratio) was introduced into a 1 mM  $\text{CuSO}_4$  aqueous solution. As shown in Figure 5a (Supplementary Video 3), initially at  $t = 0$  min, PS particles are aligned by and follow the shear flow. Then after applying the voltage, PS particles move toward the circular anode and gradually are aggregated (brighter region in the image) behind the anode in the downstream. This aggregation effect becomes more obvious at a higher voltage and lower flow rate (Figure 5b–d).

Also, as presented in Figure 5e (Supplementary Video 4), the cells of *Chlorella* sp. are initially uniformly dispersed in the aqueous solution at  $t = 0$  min (unicellular green algae, 8  $\mu\text{m}$ , FACHB-10, Freshwater Algae Culture Collection at the Institute of Hydrobiology, National Aquatic Biological Resource Center, China). Afterward, under the applied voltage, cells gradually aggregated behind the anode downstream at  $t = 15$  min.

## DISCUSSIONS

The main features and advantages of the line-charge electrode configuration presented in this work for ion enrichment in water treatment are as follows. First, the device operates based on concentration polarization between electrodes, thereby eliminating the need for a membrane. Second, it demonstrates exceptional ion enrichment efficiency ( $f_{enrich} > 15$ ). Third, the enrichment efficiency can be controlled by key physical parameters such as voltage and flow rate. Finally, the device also offers multifunctionality by enabling the removal of plastic particles and cells.

In summary, we report an extraordinary concentration enrichment mediated by a line charge down to a reduced length scale of tens of micrometers, accompanied by cation separation and extraction under continuous shear flow. Experimental observations of the spatiotemporal evolution for solute concentration within a microfluidic-based electrochemical device demonstrate a remarkable enrichment factor across various operational conditions, including geometry length scale, applied voltages, and flow rates. Both numerical simulations and scaling analyses elucidate the trade-offs between key physical parameters, providing guidance for optimizing enrichment performance. Furthermore, within the device, we have determined the preferential cation enrichment and depletion in multicomponent electrolytes and the effective removal of contaminants such as plastic particles in an aqueous solution and cells in biological samples. This portable water purification concept may extend options for drinking water access alongside large-scale desalination, including in disaster response or infrastructure-constrained environments.

## ASSOCIATED CONTENT

### Data Availability Statement

Essential data are fully provided in the main text and the Supporting Information.

### Supporting Information

The Supporting Information is available free of charge at <https://pubs.acs.org/doi/10.1021/acs.nanolett.5c04366>.

Video S1. Concentration evolution in experiments (MP4)

Video S2. Concentration evolution in simulations (MP4)

Video S3. Spatiotemporal evolution of particle removal (MP4)

Video S4. Spatiotemporal evolution of cell removal (MP4)

Experimental methods, numerical simulations, and scaling analysis (PDF)

## AUTHOR INFORMATION

### Corresponding Authors

**Moran Wang** – Department of Engineering Mechanics, Tsinghua University, Beijing 100084, China; Email: [mrwang@tsinghua.edu.cn](mailto:mrwang@tsinghua.edu.cn)

**Daosheng Deng** – Department of Aeronautics and Astronautics, College of Intelligent Robotics and Advanced Manufacturing, Fudan University, Shanghai 200433, China; [orcid.org/0000-0002-4203-5119](https://orcid.org/0000-0002-4203-5119); Email: [dsdeng@fudan.edu.cn](mailto:dsdeng@fudan.edu.cn)

### Authors

**Peng Huo** – Department of Aeronautics and Astronautics, College of Intelligent Robotics and Advanced Manufacturing, Fudan University, Shanghai 200433, China

**Wei Liu** – Department of Engineering Mechanics, Tsinghua University, Beijing 100084, China; [orcid.org/0000-0003-0844-0804](https://orcid.org/0000-0003-0844-0804)

**Zhibo Gu** – Department of Aeronautics and Astronautics, College of Intelligent Robotics and Advanced Manufacturing, Fudan University, Shanghai 200433, China

Complete contact information is available at:

<https://pubs.acs.org/10.1021/acs.nanolett.5c04366>

### Author Contributions

<sup>#</sup>P.H. and W.L. contributed equally to this work; P.H. carried out experiments, W.L. performed simulations; P.H., W.L., Z.G., M.W., and D.D. discussed the results; P.H., W.L., M.W., and D.D. wrote the paper. D.D. conceived the idea and supervised the project.

### Notes

The authors declare the following competing financial interest(s): D.D., P.H., and Z.G. are inventors on a filed Chinese patent application (CN2024109363894) related to the water treatment technology and method reported in this work.

## ACKNOWLEDGMENTS

D.D. appreciates the fruitful discussions with Boris Zaltzman, Isaak Rubinstein, and Martin Bazant. W.L. acknowledges China Postdoctoral Science Foundation (No. 2023M741970) and the Postdoctoral Fellowship Program of CPSF (No. GZB20230361); M.W. acknowledges the National Natural Science Foundation of China (Grant No. 12272207); D.D. acknowledges the National Natural Science Foundation of China (Grant No. 12272098).

## REFERENCES

- (1) Shannon, M. A.; Bohn, P. W.; Elimelech, M.; Georgiadis, J. G.; Marinas, B. J.; Mayes, A. M. Science and technology for water purification in the coming decades. *Nature* **2008**, *452*, 301.
- (2) Elimelech, M.; Phillip, W. A. The future of seawater desalination: Energy, technology, and the environment. *Science* **2011**, *333*, 721.
- (3) Schoch, R. B.; Han, J.; Renaud, P. Transport phenomena in nanofluidics. *Rev. Mod. Phys.* **2008**, *80*, 839.
- (4) Alkhadra, M. A.; et al. Electrochemical methods for water purification, ion separations, and energy conversion. *Chem. Rev.* **2022**, *122*, 13547.
- (5) Werber, J. R.; Osuji, C. O.; Elimelech, M. Materials for next-generation desalination and water purification membranes. *Nat. Rev. Mater.* **2016**, *1*, 16018.
- (6) Park, H. B.; Kamcev, J.; Robeson, L. M.; Elimelech, M.; Freeman, B. D. Maximizing the right stuff: The trade-off between membrane permeability and selectivity. *Science* **2017**, *356*, eaab0530.
- (7) Yao, Y. J.; et al. More resilient polyester membranes for high-performance reverse osmosis desalination. *Science* **2024**, *384*, 333.
- (8) Amy, G.; Ghaffour, N.; Li, Z. Y.; Francis, L.; Linares, R. V.; Missimer, T.; Lattemann, S. Membrane-based seawater desalination. *Desalination* **2017**, *401*, 16.
- (9) Porada, S.; Zhao, R.; van der Wal, A.; Presser, V.; Biesheuvel, P. M. Review on the science and technology of water desalination by capacitive deionization. *Prog. Mater. Sci.* **2013**, *58*, 1388.
- (10) Suss, M. E.; Porada, S.; Sun, X.; Biesheuvel, P. M.; Yoon, J.; Presser, V. Water desalination via capacitive deionization: what is it and what can we expect from it? *Energy Environ. Sci.* **2015**, *8*, 2296.
- (11) Srimuk, P.; Su, X.; Yoon, J.; Aurbach, D.; Presser, V. Charge-transfer materials for electrochemical water desalination, ion separation and the recovery of elements. *Nat. Rev. Mater.* **2020**, *5*, 517.
- (12) Shin, S.; Shardt, O.; Warren, P. B.; Stone, H. A. Membraneless water filtration using CO<sub>2</sub>. *Nat. Commun.* **2017**, *8*, 15181.
- (13) Probstein, R. F. *Physicochemical Hydrodynamics*; Wiley, New York, 2003.
- (14) Sonin, A. A.; Probstein, R. F. A hydrodynamic theory of desalination by electrodialysis. *Desalination* **1968**, *5*, 293.
- (15) Humplik, T.; et al. Nanostructured materials for water desalination. *Nanotechnol* **2011**, *22*, 292001.
- (16) Kim, S. J.; Ko, S. H.; Kang, K. H.; Han, J. Direct seawater desalination by ion concentration polarization. *Nat. Nanotechnol.* **2010**, *5*, 297.
- (17) Yang, Y. B.; et al. Large-area graphene-nanomesh/carbon-nanotube hybrid membranes for ionic and molecular nanofiltration. *Science* **2019**, *364*, 1057.
- (18) Levich, V. G. The theory of concentration polarization. I. *Acta Physicochim. URSS* **1942**, *17*, 257.
- (19) Levich, V. G. Theory of concentration polarization. II. Steady-state regime. *Acta Physicochim. URSS* **1944**, *19*, 117.
- (20) Levich, V. G. *Physicochemical Hydrodynamics*; Prentice-Hall, Inc., 1962.
- (21) Rubinstein, I.; Zaltzman, B. Electro-osmotically induced convection at a permselective membrane. *Phys. Rev. E* **2000**, *62*, 2238.
- (22) Zaltzman, B.; Rubinstein, I. Electro-osmotic slip and electroconvective instability. *J. Fluid Mech.* **2007**, *579*, 173.
- (23) Rubinstein, S. M.; et al. Direct observation of a nonequilibrium electro-osmotic instability. *Phys. Rev. Lett.* **2008**, *101*, 236101.
- (24) Yossifon, G.; Chang, H.-C. Selection of nonequilibrium overlimiting currents: Universal depletion layer formation dynamics and vortex instability. *Phys. Rev. Lett.* **2008**, *101*, 254501.
- (25) Wang, Y. C.; Stevens, A. L.; Han, J. Million-fold preconcentration of proteins and peptides by nanofluidic filter. *Anal. Chem.* **2005**, *77*, 4293.
- (26) Ouyang, W.; Ye, X. H.; Li, Z. R.; Han, J. Deciphering ion concentration polarization-based electrokinetic molecular concentration at the micro-nanofluidic interface: theoretical limits and scaling laws. *Nanoscale* **2018**, *10*, 15187.
- (27) Zangle, T. A.; Mani, A.; Santiago, J. G. Theory and experiments of concentration polarization and ion focusing at microchannel and nanochannel interfaces. *Chem. Soc. Rev.* **2010**, *39*, 1014.
- (28) Dydek, E. V.; Zaltzman, B.; Rubinstein, I.; Deng, D. S.; Mani, A.; Bazant, M. Z. Overlimiting current in a microchannel. *Phys. Rev. Lett.* **2011**, *107*, 118301.
- (29) Mani, A.; Bazant, M. Z. Deionization shocks in microstructures. *Phys. Rev. E* **2011**, *84*, 061504.
- (30) Deng, D. S.; Dydek, E. V.; Schlumpberger, S.; Han, J. H.; Mani, A.; Zaltzman, B.; Bazant, M. Z. Overlimiting current and shock electrodialysis in porous media. *Langmuir* **2013**, *29*, 16167.

- (31) Deng, D. S.; Aouad, W.; Braff, W.; Schlumpberger, S.; Suss, M.; Bazant, M. water purification by shock electrodialysis: deionization, filtration, separation, and disinfection. *Desalination* **2015**, *357*, 77.
- (32) Anand, R. K.; et al. Bipolar electrodes: A useful tool for concentration, separation, and detection of analytes in micro-electrochemical systems. *Anal. Chem.* **2010**, *82*, 8766.
- (33) Fosdick, S. E.; Knust, K. N.; Scida, K.; Crooks, R. M. Bipolar electrochemistry. *Angew. Chem., Int. Ed.* **2013**, *52*, 10438.
- (34) Anand, R. K.; Sheridan, E.; Knust, K. N.; Crooks, R. M. Bipolar electrode focusing: Faradaic ion concentration polarization. *Anal. Chem.* **2011**, *83*, 2351.
- (35) Sheridan, E.; Hlushkou, D.; Knust, K. N.; Tallarek, U.; Crooks, R. M. Enrichment of cations via bipolar electrode focusing. *Anal. Chem.* **2012**, *84*, 7393.
- (36) Li, G. J.; Archer, L. A.; Koch, D. L. Electroconvection in a viscoelastic electrolyte. *Phys. Rev. Lett.* **2019**, *122*, 124501.
- (37) Shi, P.; Liu, W. Length-dependent instability of shear electroconvective flow: From electroconvective instability to Rayleigh-Benard instability. *J. Appl. Phys.* **2018**, *124*, 204304.
- (38) Liu, W.; Zhou, Y. T.; Shi, P. P. Critical selection of shear sheltering in electroconvective flow from chaotic to steady state. *J. Fluid Mech.* **2022**, *946*, A3.
- (39) Mani, A.; Wang, K. M. Electroconvection near electrochemical interfaces: Experiments, modeling, and computation. *Annu. Rev. Fluid Mech.* **2020**, *52*, 509.
- (40) Xu, B.; et al. Electro-osmotic instability of concentration enrichment in curved geometries for an aqueous electrolyte. *Phys. Rev. Fluids* **2020**, *5*, 091701R.
- (41) The typical parameters are the shear velocity  $u_{shear} = Q_m/(hl) \sim 1$  mm/s ( $Q_m \sim 0.1$   $\mu$ L/s, the thickness of the device  $h = 30$   $\mu$ m, and the length between two parallel cathodes  $l = 4$  mm), the diameter of the central anode  $d \sim 200$   $\mu$ m, and the diffusion coefficient  $D \sim 10^3$   $\mu$ m<sup>2</sup>/s.
- (42) Kwak, R.; Pham, V. S.; Lim, K. M.; Han, J. Shear flow of an electrically charged fluid by ion concentration polarization: scaling laws for electroconvective vortices. *Phys. Rev. Lett.* **2013**, *110*, 114501.
- (43) Ma, M. C.; Li, G.; Chen, X.; Archer, L. A.; Wan, J. Suppression of dendrite growth by cross-flow in microfluidics. *Sci. Adv.* **2021**, *7*, eabf6941.
- (44) Liu, W.; Zhou, Y.; Shi, P. Effect of concentration polarization on permselectivity. *J. Fluid Mech.* **2022**, *946*, A3.
- (45) Tian, H.; Luo, J.; Mu, J.; Liu, B. Insight into the mechanisms of efficient selective removal of Pb<sup>2+</sup> from wastewater by nano-flowered MoS<sub>2</sub>/NHCS electrodes. *J. Environ. Chem. Eng.* **2024**, *12*, 113039.
- (46) Esalah, J.; Husein, M. M. Removal of Heavy Metals from Aqueous Solutions by Precipitation-Filtration Using Novel Organo-Phosphorus Ligands. *Sep. Purif. Technol.* **2008**, *43*, 3461.
- (47) Zhang, B.; Du, X.; Hao, X.; Gao, F.; Zhang, D.; Liu, C.; Guan, G. A novel potential-triggered SBA-15/PANI/PSS composite film for selective removal of lead ions from wastewater. *J. Solid State Electrochem.* **2018**, *22*, 2473.
- (48) Tian, H.; Alkhadra, M. A.; Conforti, K. M.; Bazant, M. Z. Continuous and Selective Removal of Lead from Drinking Water by Shock Electrodialysis. *ACS EST Water* **2021**, *1*, 2269.
- (49) Li, L.; et al. Effective uptake of submicrometre plastics by crop plants via a crack-entry mode. *Nat. Sustain.* **2020**, *3*, 929.
- (50) MacLeod, M.; Arp, H. P. H.; Tekman, M. B.; Jahnke, A. The global threat from plastic pollution. *Science* **2021**, *373*, 61.
- (51) Moon, S.; et al. Direct observation and identification of nanoplastics in ocean water. *Sci. Adv.* **2024**, *10*, eadh1675.
- (52) Hur, S. C.; Mach, A. J.; Carlo, D. D. High-throughput size-based rare cell enrichment using microscale vortices. *Biomicrofluidics* **2011**, *5*, 22206.
- (53) Sutermeister, B. A.; Darling, E. M. Considerations for high-yield, high-throughput cell enrichment: fluorescence versus magnetic sorting. *Sci. Rep.* **2019**, *9*, 227.